

ANALYSIS OF GRAVITY AND AEROMAGNETIC DATA,
SAN FRANCISCO MOUNTAINS AND VICINITY,
SOUTHWESTERN UTAH

by J. W. Schmoker

UTAH GEOLOGICAL AND MINERALOGICAL SURVEY
affiliated with
THE COLLEGE OF MINES AND MINERAL INDUSTRIES
University of Utah, Salt Lake City, Utah



BULLETIN 98

PRICE \$2.00

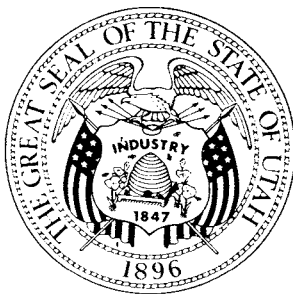
NOVEMBER 1972

B98

ANALYSIS OF GRAVITY AND AEROMAGNETIC DATA,
SAN FRANCISCO MOUNTAINS AND VICINITY,
SOUTHWESTERN UTAH

by J. W. Schmoker

UTAH GEOLOGICAL AND MINERALOGICAL SURVEY
affiliated with
THE COLLEGE OF MINES AND MINERAL INDUSTRIES
University of Utah, Salt Lake City, Utah



CONTENTS

	Page
Abstract	1
Introduction	1
General Setting	1
Magnetic Susceptibility of Rocks	2
Remanent Magnetization	4
Rock Density	5
Aeromagnetic Data	5
Introduction	5
Regional and Residual Maps	5
Observations	6
Model Studies of Intrusive Structure	7
Regional Geologic Implications	8
Gravity Survey	11
Introduction	11
Observations (Residual Gravity Map)	11
Interpretation of Selected Residual Gravity Profiles	15
Relative Age of Intrusive Emplacement	19
Interpretation of Regional Gravity Anomalies	19
Summary and Conclusions	23
Acknowledgments	23
References	23
ILLUSTRATIONS	
Figure	
1. Index map of Utah showing location of study area	2
2. Generalized geologic map of the San Francisco Mountains vicinity, southwestern Utah	3
3. Aeromagnetic map of the San Francisco Mountains vicinity, southwestern Utah	4
4. Portion of ground magnetic traverse	5
5. 15*15 running average regional map of the aeromagnetic data	6
6. 15*15 running average residual map of the aeromagnetic data	7
7. Perspective drawing of the regional igneous model	8
8. Perspective drawing of the residual igneous model	8
9. Total-intensity magnetic field generated by the regional igneous model	9
10. Total-intensity magnetic field generated by the residual igneous model	10
11. Total-intensity magnetic field generated by the total igneous model	11
12. Comparison of observed regional aeromagnetic data and the anomalies computed over horizontal plates	12
13. Outcrop pattern of intrusive rocks in southwestern Utah	12
14. 13*13 running average residual map of the Bouguer anomaly gravity data	13
15. 13*13 running average regional map of the Bouguer anomaly gravity data	14
16. Residual gravity profile AA'	16
17. Residual gravity profile BB'	17
18. Residual gravity profile CC'	18
19. Regional gravity data with the postulated gravity effect of the regional intrusive body removed	20
20. Sketch showing relationship of the regional intrusive model to the horizontal plate representing north side of postulated fault zone	21
21. Regional gravity data minus the possible gravity effects of both the regional intrusive body and the postulated high-density plate	22
Table	
1. Summary of susceptibility measurements	2
2. Maximum depths of fill for the Wah Wah, Big Wash and Milford Valley grabens	19

ANALYSIS OF GRAVITY AND AEROMAGNETIC DATA, SAN FRANCISCO MOUNTAINS AND VICINITY, SOUTHWESTERN UTAH

by James W. Schmoker¹

ABSTRACT

Regional geologic structures in the San Francisco Mountains vicinity, southwestern Utah, are investigated using aeromagnetic and gravimetric data.

Aeromagnetic data indicate a buried Tertiary pluton whose north boundary runs east to west across the study area and which extends beyond the coverage of the aeromagnetic map to the east, south and west. Local cupolas extend upward from the main igneous body. A three-dimensional model is developed with a digital computer for the distribution of the magnetic rocks in the area. These model studies show that the pluton is tabular, about 5 miles thick and has a near-vertical and linear north edge which may have resulted from the structural control exerted by an east-west trending fault zone.

The Bouguer gravity anomalies reflect horst and graben structures typical of the Basin and Range Province and indicate a density contrast of +.10 grams per cc is associated with the local intrusive cupolas. Three interpretive east-west geologic cross sections are developed which reproduce observed residual gravity anomalies.

The regional gravity data are interpreted to show the effect of three regional structures:

1. An underlying intrusive body.
2. An east-west fault zone bounding the intrusive body on the north.
3. A continuation of Basin and Range structure at depths exceeding two miles.

INTRODUCTION

The United States Geological Survey published the "Aeromagnetic map of the San Francisco Mountains and vicinity, southwestern Utah" (USGS, 1966a) and placed on open file the "Complete Bouguer gravity anomaly map of the San Francisco Mountains vicinity, Beaver and Millard counties, Utah" (USGS, 1966b). In this paper, an interpretation of the regional geology of the San Francisco Mountains vicinity is developed,

based largely on the geophysical data provided by these two maps.

The San Francisco Mountains district is a 980-square-mile rectangle bounded by the north latitudes of 38°15' and 38°45' and the west longitudes of 113°100' and 113°30'. The area covers parts of Beaver and Millard counties in southwestern Utah (figure 1). Base maps for the 30-minute rectangle are the four U. S. Geological Survey 15-minute topographic quadrangle maps of Frisco Peak (1960), Beaver Lake Mountains (1960), Frisco (1959) and Milford (1958). The Utah Geological and Mineralogical Survey sponsored several exploration and mapping projects in this area, results of which are available as published reports.

GENERAL SETTING

The San Francisco Mountains area lies near the east margin of the Great Basin and the physiography of the area is similar to that of other parts of the Basin and Range geologic province. Elevations range from 4,500 feet along the north central boundary to 9,600 feet in the San Francisco Mountains. Except for the easternmost portion near Milford, human habitation is almost completely lacking. From west to east the study area includes the east edge of the Wah Wah Mountains, the San Francisco Mountains and a chain of north-south aligned ranges consisting of the Beaver Lake Mountains to the north, the Rocky Range and the Star Range.

The complex structural and stratigraphic history of the Great Basin has been investigated by many authors: Butler (1913), Butler and others (1920), Boardman (1954), Roberts and others (1958), Harris (1959), Jaffe and others (1959), Mackin (1960a and b), Roberts (1960), Eardley (1962) and Armstrong (1968).

Surface features reflect in large part the block faulting and igneous activity characterizing the present Basin and Range Province. The nature of Basin and Range structure was first properly described by Gilbert (1874) and was discussed in detail by Davis (1925), Gilbert (1928), Nolan (1943), Moore (1960) and Mackin (1960a).

Figure 2 shows the generalized geology of the area, modified from Hintze's (1963) Geologic Map of Southwestern Utah.

¹ Atlantic Richfield Company, P. O. Box 2819, Dallas, Texas 75221.

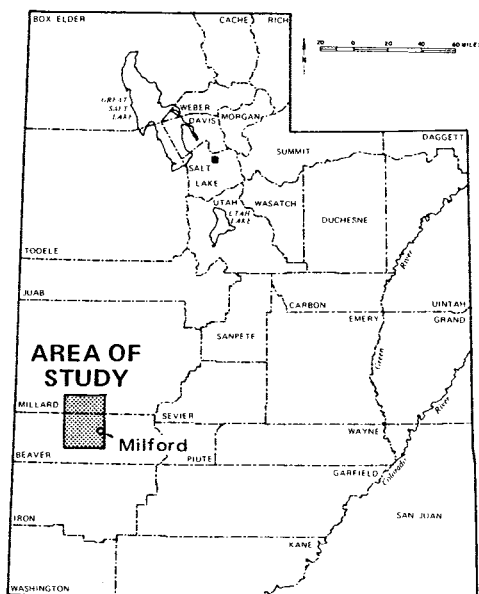


Figure 1. Index map of Utah showing the location of the study area.

MAGNETIC SUSCEPTIBILITY OF ROCKS

The magnetic susceptibilities of samples representing most of the outcropping rock types in the area were measured to determine which rock units might generate magnetic anomalies. Table 1 summarizes these measurements. Individual susceptibility determinations could be repeated to $\pm .000035$ cgs units.

The consolidated sedimentary rocks of the Cordilleran miogeosyncline contain little ferrous material and have low susceptibilities. The samples of unconsolidated alluvium have significantly higher susceptibilities, although their magnetic effect is still of secondary importance. Magnetite in the alluvium is not easily destroyed by weathering and appears to have been eroded from the igneous rocks of the area.

Samples from fissure-replacement and contact-zone mineralization were taken from areas too small to noticeably influence the aeromagnetic data (obtained 3,000 to 4,000 feet above the ground surface), but which could be important to ground-magnetic surveys. Mineralization of the fissure-replacement type, with an average susceptibility of .000160 cgs units, probably would not be detectable in this area using ordinary ground-magnetic-surveying techniques. In contrast, samples from contact zones, selected from areas where copper mineralization was present, contained so much magnetite that susceptibilities exceeded the range of the available susceptibility bridge. Susceptibilities of these samples were estimated on the basis of percent magnetite content.

The aeromagnetic map (figure 3) does not appear to be influenced by surface volcanics and susceptibility measurements confirm that the magnetization of the volcanics is low. Most of the volcanics present are pyroclastic ignimbrites, which tend to have minimal magnetization (Mabey and others, 1964).

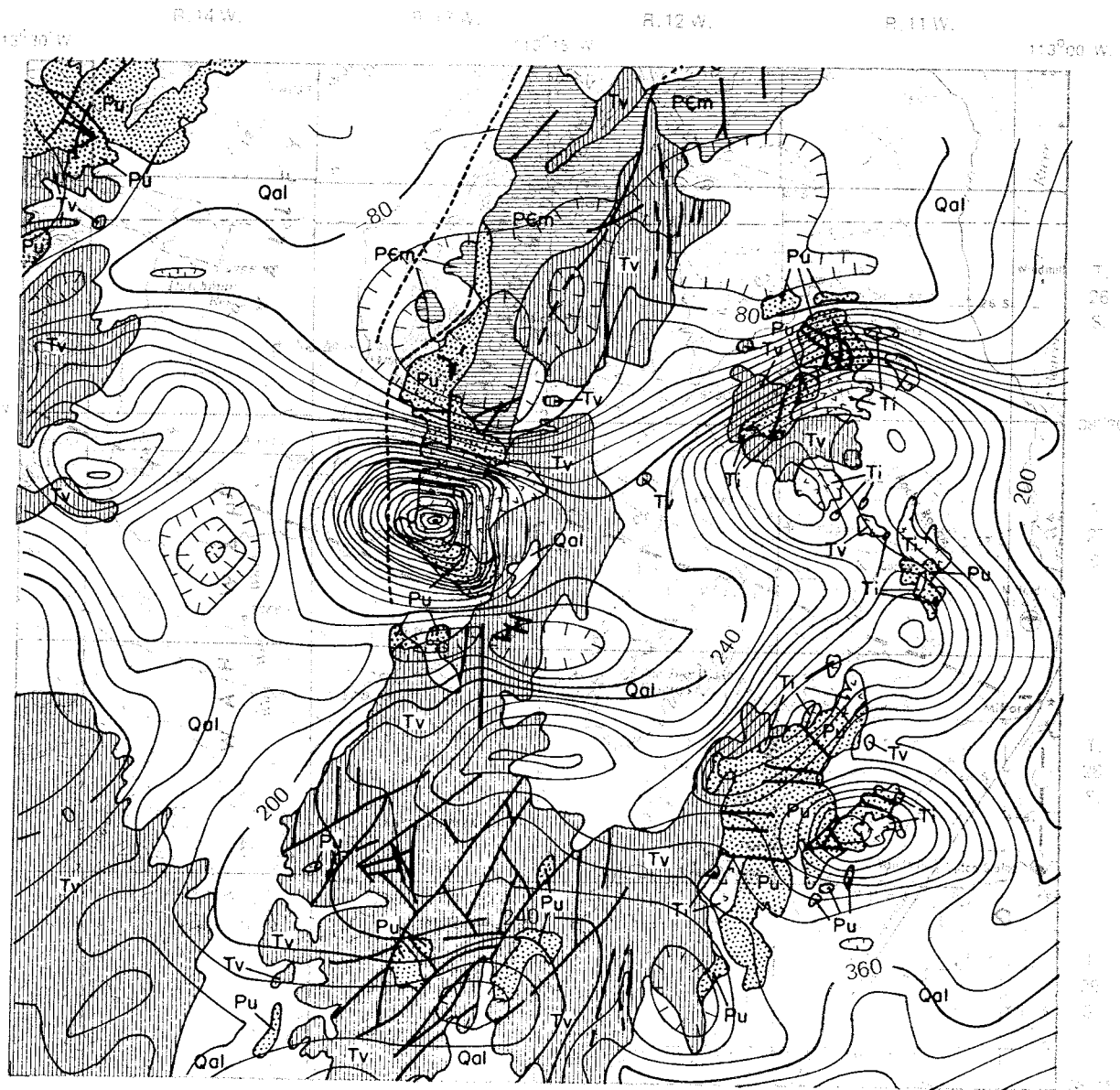
Intrusive rocks have significant susceptibilities throughout the area. Fourteen samples, representing most of the intrusive exposures, have susceptibilities ranging from .002370 to .004400 cgs units, with an average value of .003450 cgs units. Table 1 lists these measurements individually. No apparent relationship exists in this limited sampling between susceptibility and intrusive location.

The variations in susceptibility among the intrusive samples measured seem characteristic of the intrusive rocks in the area and occur over intervals as small as a few tens of feet. Figure 4 shows a portion of a vertical-field ground-magnetic profile across an intrusive

Table 1. Summary of susceptibility measurements.

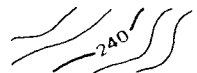
Rock Type	Avg. Susceptibility (cgs units)	Number of Samples
1) Consolidated sedimentary rocks—limestone and quartzite	.000040	5
2) Alluvium	.000280	3
3) Fissure-replacement mineralization	.000160	7
4) Contact-zone mineralization	~.100000	4
5) Extrusive igneous rocks—acidic	.000140	4
6) Intrusive igneous rocks—quartz, monzonite and granodiorite	.003450	14

Individual Intrusive Rock Susceptibility Measurements (cgs units)	Sample Location (figure 2)
.003910	Star Range
.002370	Star Range
.003020	Star Range
.004050	Star Range
.003020	Star Range
.004400	Star Range
.002960	Star Range
.003880	Star Range
.004130	San Francisco Mountains
.003320	San Francisco Mountains
.003790	Beaver Lake Mountains
.002580	Beaver Lake Mountains
.003110	Rocky Range
.003760	Rocky Range



2 0 2 4 6 8 Miles

Geology from "Geologic map of southwestern Utah" (Hintze, 1963).



Contour Interval = 40 gammas

Aeromagnetic contours with a plane regional gradient corresponding to the gradient of the earth's main field removed, from the "Aeromagnetic map of the San Francisco Mountains and vicinity, southwestern Utah" (U. S. Geol. Survey, 1966a).

AA', BB' and CC' are profiles along which gravity data (U. S. Geol. Survey, 1966b) were interpreted.

- Qal Quaternary alluvium, undifferentiated
- Ti Tertiary intrusive rocks
- Tv Tertiary extrusive rocks
- Pu Cambrian to Jurassic sedimentary rocks
- PCm Precambrian metasedimentary rocks

--- Fault (dashed where probable, dotted where concealed)

Figure 2. Generalized geologic map of the San Francisco Mountains vicinity, southwestern Utah.

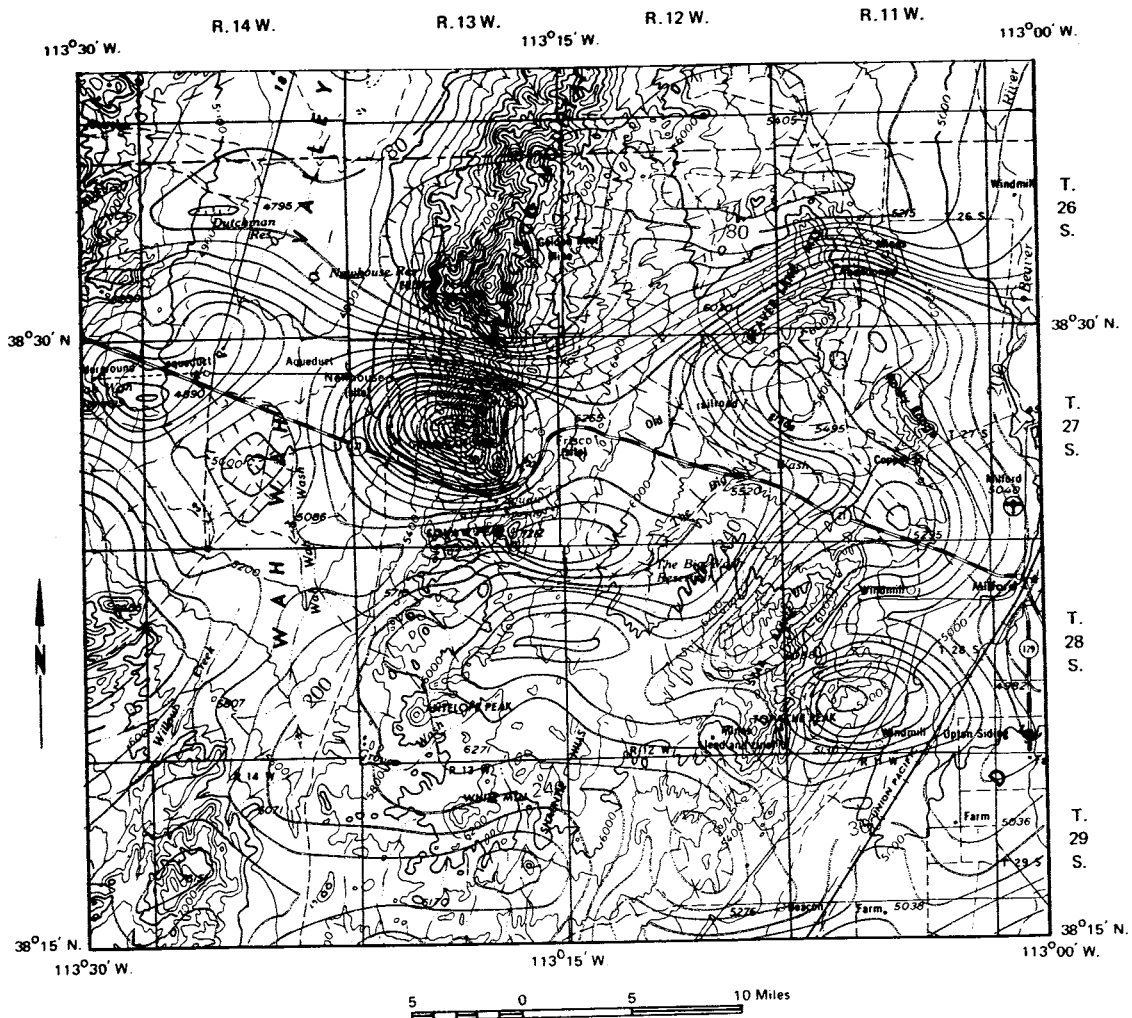


Figure 3. Aeromagnetic map of the San Francisco Mountains vicinity, southwestern Utah. A plane regional gradient corresponding to the gradient of the earth's main field was removed. Contour interval = 40 gammas.

exposure in the Star Range and demonstrates the irregular magnetization of the quartz monzonite.

Six areas of intrusive outcrop are shown on the geologic map (figure 2), five of which have definite expression on the aeromagnetic map. The southernmost intrusive outcrop, in the Star Range, has no aeromagnetic anomaly. Susceptibility measurements of samples from this outcrop (which were not included in table 1) give an average susceptibility of .000400 cgs units, at least eight times lower than that of the other intrusive outcrops. Ground-magnetic profiles confirm that this igneous body has essentially no magnetic expression. Mabey and others (1964) note that an intrusive of similar age, the Bingham stock, southwest of Salt Lake City, has no appreciable magnetic expression, presumably because of the destruction of magnetite by hydrothermal alteration.

REMANENT MAGNETIZATION

In the Basin and Range Province, directions of remanent magnetization of igneous rocks tend to fall into two groups: a normal group where remanent magnetization parallels the present geomagnetic field and a reversed group where remanent vectors are directed opposite to the present earth's field (Doell and Cox, 1962). The two directions are presumed to arise from changes in the polarity of the earth's main field; at least twenty polarity changes are suggested since Eocene time (Doell and Cox, 1962).

No measurements of remanent magnetization are available from the San Francisco Mountains area. In all subsequent analyses of magnetic field data, the magnetization vector was assumed to parallel the earth's main field.

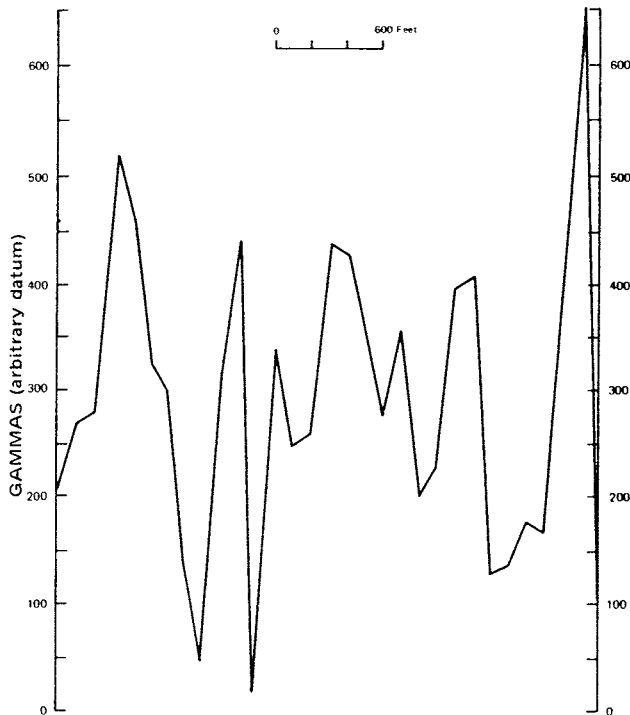


Figure 4. Portion of a ground magnetic traverse over a quartz monzonite intrusive exposure showing the irregular nature of the magnetization. Station spacing was 100 feet.

ROCK DENSITY

Densities of 2.70 and 2.25 grams per cc for consolidated Paleozoic and unconsolidated Cenozoic rocks, respectively, have proven applicable in the Basin and Range Province (Mabey and Morris, 1967). Cenozoic volcanic rocks have average densities of 2.45 grams per cc and Tertiary intrusive rock densities range from 2.60 to 2.80 grams per cc (Carlson and Mabey, 1963). Metamorphosed Early Precambrian rocks have densities averaging 2.86 grams per cc (Mabey, 1963), but such rocks are not exposed in the study area. Late Precambrian rocks exposed in the northern San Francisco Mountains are not highly altered and have little if any density contrast with the Paleozoic rocks (Mabey, 1963; Carlson and Mabey, 1963).

AEROMAGNETIC DATA

Introduction

An aeromagnetic survey of the San Francisco Mountains and adjacent areas compiled by the U. S. Geological Survey (USGS, 1966a) covers an area of about 980 square miles—28 miles in an east-west direction and 35 miles in a north-south direction. It was flown 9,000 feet above sea level along east-west flight lines with an average separation of 1 mile. Total-intensity magnetic-field contours are given at 20-gamma intervals.

A plane regional field corresponding to the gradient of the earth's main magnetic field of 7.6 gammas per mile, increasing in the direction N 26° E (U. S. Coast and Geodetic Survey, 1955), was removed from the original data. Figure 2 shows the resulting magnetic field superposed on the geologic map of the area. After removal of this gradient, the north 9 miles of the map showed only an increasing magnetic gradient of about 10 gammas per mile toward the north, corresponding to a slow recovery from the large magnetic low to the south. Because this part of the magnetic map was essentially featureless, subsequent interpretations deal mainly with the south 26 miles of the original map.

Figure 3 shows the south three-fourths of the aeromagnetic data contoured at 40-gamma intervals with the gradient of the earth's main field removed. This map was machine-contoured from a digitized data set.

Regional and Residual Maps

The separation of gravity and magnetic maps into regional and residual components long has been an accepted step in the interpretation of potential field data. The basic ambiguity of such separations (for example, Skeels, 1947 and Nettleton, 1954) has led to the development of numerous techniques for the extraction of regional fields. The final selection of a method to obtain regional and residual separations must be based on subjective judgment of the geological significance of the maps produced and the cost of the method in terms of labor and facilities. After considering and testing three methods for regional-residual separations—least-square polynomial fitting, wave-length filtering and running averages—the running average method was judged most suitable for this particular investigation.

In the running average method of obtaining regional surfaces, mean values for specified overlapping portions of the observed data are determined. For the gridded data of figure 3, the data in a square about a given point of application with sides of N data points were summed and divided by N^2 to obtain regional or smoothed values. The notation $N*N$ running average indicates that data in squares having sides of N data points were averaged.

Of the various running average operators applied to the aeromagnetic data, the $15*15$ operator appears, subjectively, to produce the most meaningful separation of the data. Figures 5 and 6 present the $15*15$ running average regional and residual maps of the aeromagnetic data. In subsequent analysis, geological explanations are provided for both the regional and

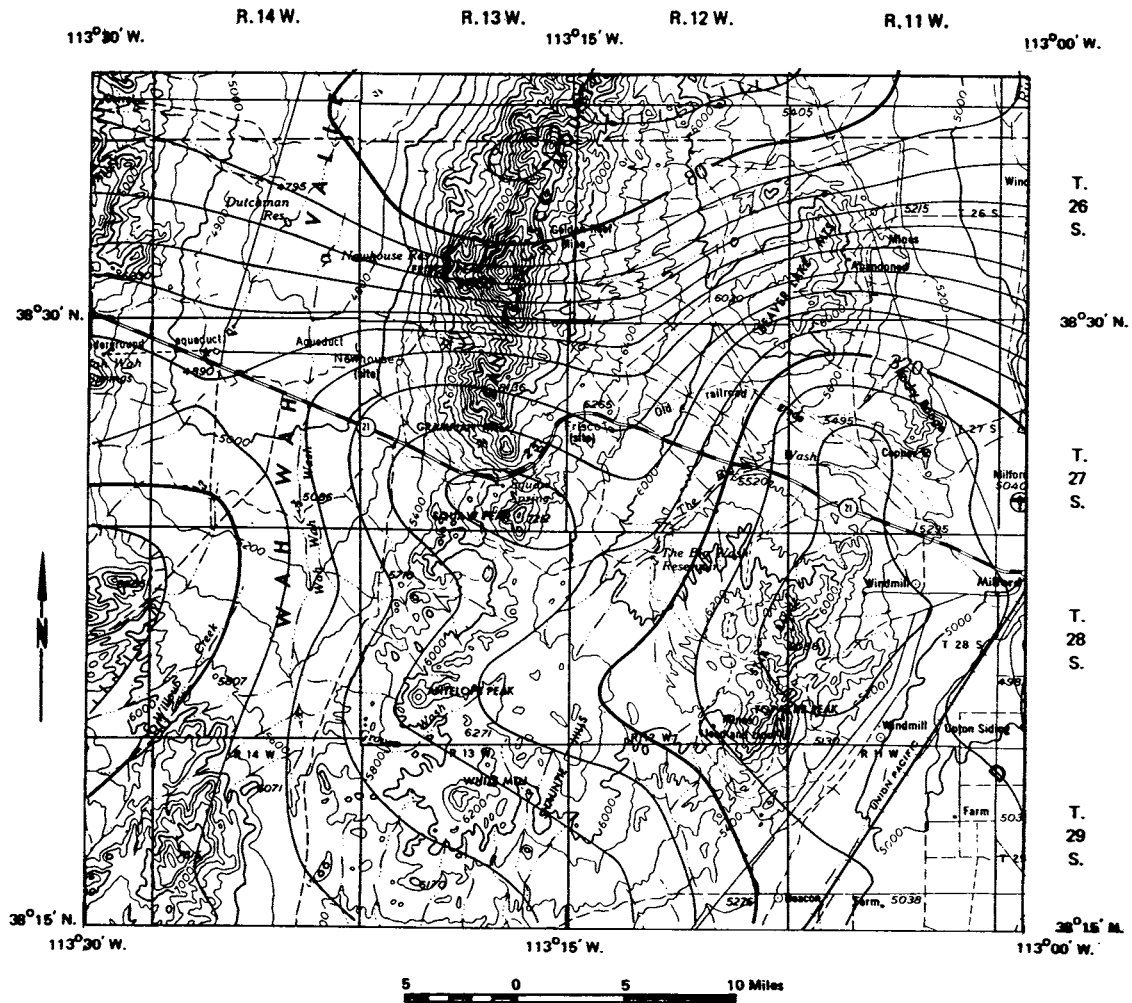


Figure 5. 15*15 running average regional map of the aeromagnetic data on figure 3. Contour interval = 40 gammas.

residual maps. Consequently, the ambiguity encountered in removing a "regional" field by an arbitrary method is avoided.

Observations

The upper 9 miles of the original aeromagnetic map are devoid of large anomalies while the lower three-fourths of the map show a considerably more disturbed magnetic field. As Affleck (1963) notes, areas of consistent magnetic character with distinct boundaries are common on magnetic surveys; such areas can be referred to as magnetic provinces. On this map, portions of two magnetic provinces appear. Figures 3, 5 and 6 include the south magnetic province.

Figure 2 shows that extrusive igneous rocks rank next to unconsolidated sediments in areal surface exposure, but have little if any magnetic expression. Apparently the few susceptibility measurements reported in table 1, which show low values of susceptibility for the volcanic rocks, are representative of the whole area.

Each of the intrusive exposures shown on figure 2, with the exception of the southernmost intrusive exposure, corresponds to a magnetic high on the residual aeromagnetic map (figure 6). The two remaining residual magnetic highs—one on the west edge of the map near Wah Wah Springs and the other south-southeast of the large anomaly just west of the site of Frisco—occur over volcanic rocks and alluvium. They too may be caused by intrusive bodies near the

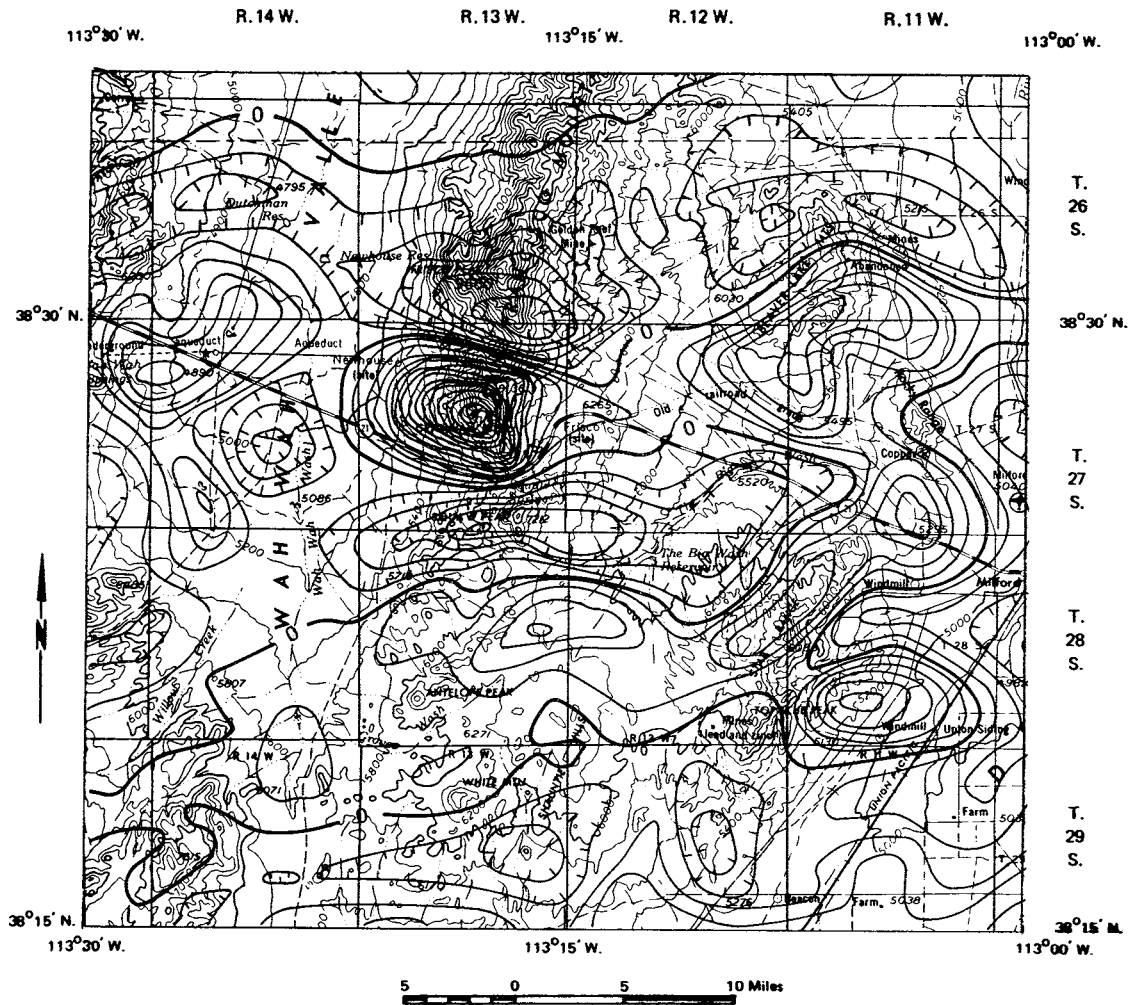


Figure 6. 15*15 running average residual map of the aeromagnetic data on figure 3. This map was obtained by subtracting the data of figure 5 from that of figure 3. Contour interval = 40 gammas.

surface which are covered by relatively thin layers of volcanics and alluvium.

The regional aeromagnetic map (figure 5) shows those magnetic features which are related to larger causative structures. One of the most striking features on the original map (figure 3) is the gradient which runs more or less linearly from east to west across the north part of the map. This feature is transverse to Basin and Range structure. On figure 3, the basic gradient has been intensified by the effect of three more local magnetic features; figure 5 shows the regional nature of this gradient. Figure 5 also shows a regional magnetic gradient decreasing from east to west in the south part of the area. The regional magnetic contours thus tend to strike east-west in the north one-third of figure 5 and north-south in the south two-thirds.

Model Studies of Intrusive Structure

The aeromagnetic data are shown to be consistent with the following geological model. The south magnetic province is the magnetic expression of an intrusive body of batholithic proportions with a north boundary extending from east to west across the north portion of the area and otherwise extending beyond the area of aeromagnetic coverage. The elevation of the top of the pluton decreases from about 2,000 feet above sea level in the east to about 11,000 feet below sea level in the west and local intrusive cupolas extend upward from the main igneous body. The pluton is distinctly tabular with a more or less uniform thickness of 5 miles and has a vertical or near-vertical north edge.

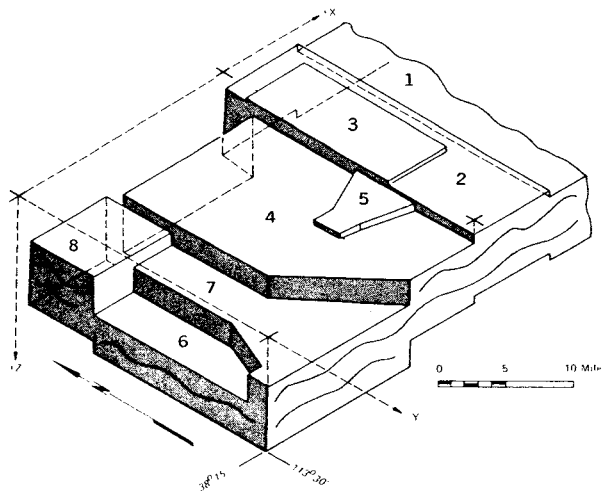


Figure 7. Perspective drawing of the regional igneous model. Numbers designate the individual plates comprising the net model. To the east, west and south, the model continues beyond the area of aeromagnetic coverage. Crosses mark the plane of the flight line.

To demonstrate that this model can reproduce the general patterns of the aeromagnetic map and to investigate the model's physical parameters, a computer program was written for the computation of the magnetic field over three-dimensional forms (after Talwani, 1965) and models for the distribution of magnetic rocks in the area were developed.

The earth's main field in the area has an approximate declination of 16 degrees (east), an inclination of 64 degrees and a total field strength of approximately 54,000 gammas (Vestine and others, 1947). These values were used in the magnetic modeling program for computing induction effects. A susceptibility of $k=.003450$ cgs units was used for all igneous models. No remanent magnetization effects were introduced.

The model developed to fit the regional aeromagnetic data of figure 5 is shown in figure 7 and consists of eight geometrically simple blocks. The north termination of the model is shown, but to the east, south and west, the aeromagnetic data did not extend to the edge of the magnetic body. Figure 9 shows the total-intensity magnetic field generated by this model at an elevation of 9,000 feet and should be compared to figure 5. The model demonstrates that the regional gradients in the observed aeromagnetic field can be generated by a large magnetic body with a steeply inclined or vertical north edge and a progressively greater depth of burial from east to west. Correlation between figures 5 and 9 is poorest in the east central area where the model is closest to the flight line. The magnetic response to geometric detail is more

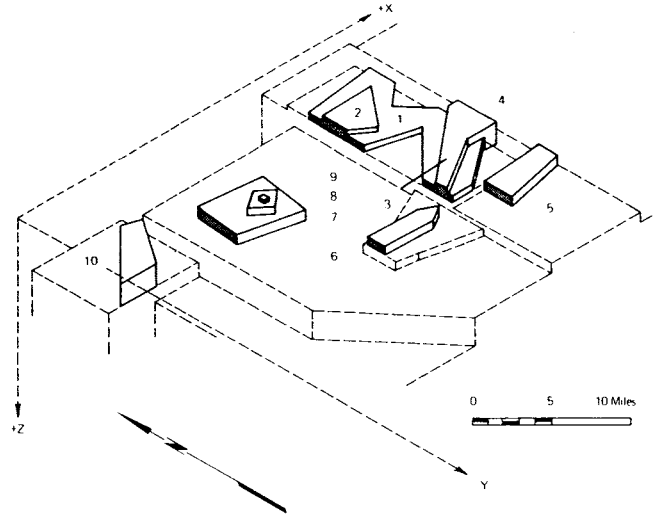


Figure 8. Perspective drawing of the residual igneous model. Numbers designate the individual plates comprising the net model. Dotted lines show the top of the regional igneous model on which the plates of the residual model lie.

pronounced in this area making it harder to fit the observed data with an idealized model.

Figure 8 shows the model designed to duplicate the residual aeromagnetic data of figure 6. Figure 10 shows the total-intensity magnetic field computed over the residual model at an elevation of 9,000 feet and should be compared to figure 6, the 15×15 running average residual map. Figure 6 has many low-amplitude closures and noses, which a model cannot easily duplicate. The model does reproduce the magnetic highs of the residual map both with respect to shape and amplitude. Severe constraints were imposed on the cupolas of the residual model. The lower extent of the cupolas was defined by the top of the regional model, while the upward extent was, in most cases, controlled by surface topography. A constant susceptibility of $k=.003450$ cgs units was prescribed. Nevertheless, the residual cupolas generated magnetic anomalies not only with the desired shapes, but with the correct amplitudes.

The magnetic field of the complete model, obtained by adding the regional and residual computed fields, is shown in figure 11 (compare to figure 3).

Regional Geologic Implications

The following discussion is based on the assumption that the distribution of magnetic material, as shown in figures 7 and 8, represents a Tertiary intrusive body of batholithic proportions. Many of the cupolas of the model correspond to outcrops of quartz

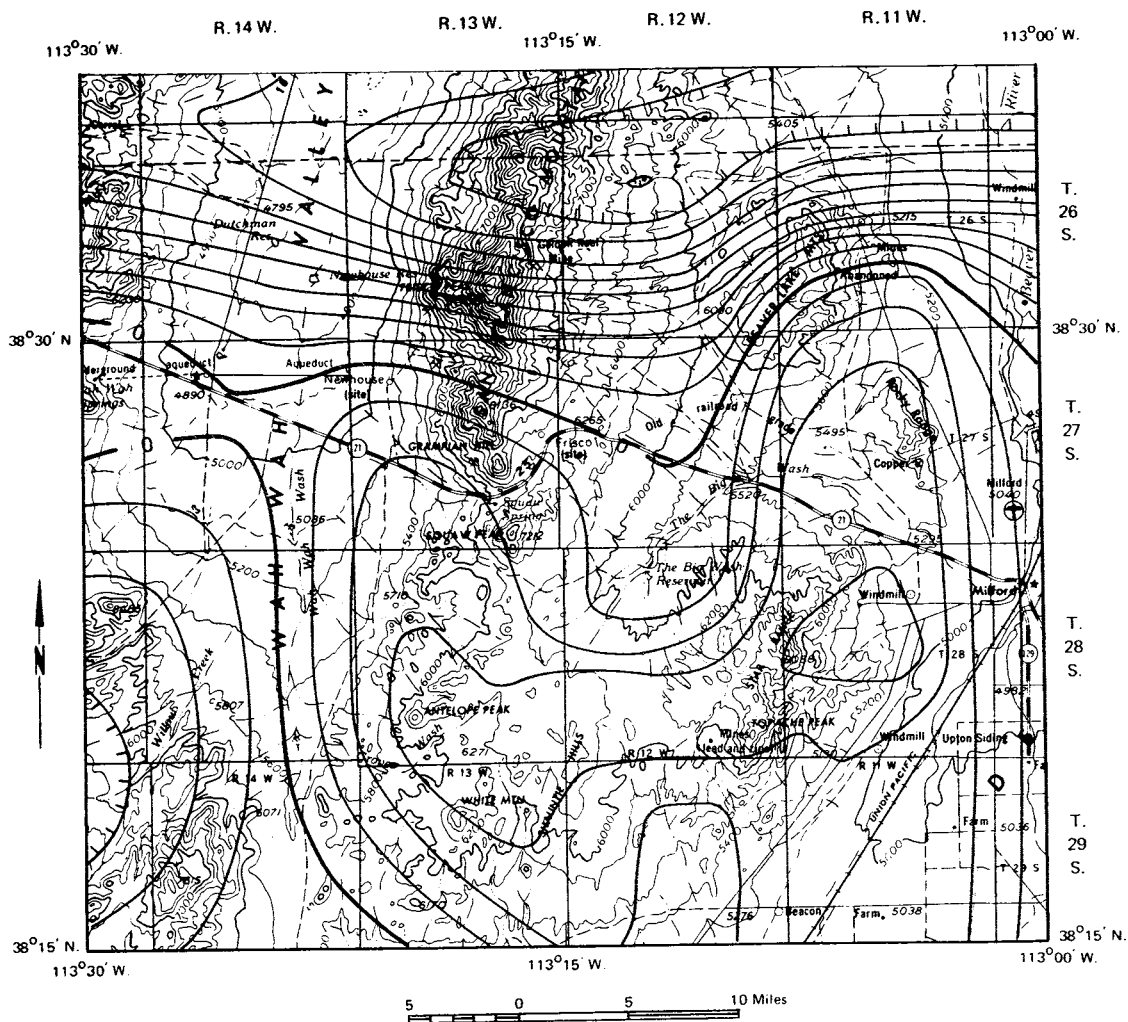


Figure 9. Total-intensity magnetic field generated by the regional igneous model. Values were computed at an elevation of 9,000 feet. This figure should be compared to figure 5. Contour interval = 40 gammas.

monzonite and granodiorite intrusive bodies of Tertiary age. The finite thickness of the regional model implies that it does not reflect susceptibility contrasts in basement rocks. Even over the exposure of Precambrian rocks in the north part of the San Francisco Mountains (figure 2), no magnetic effect of basement rocks is recognized. Aeromagnetic surveys in the Tintic area to the north (Mabey and Morris, 1967) and the Iron Springs district to the south (Blank and Mackin, 1967) are similarly interpreted in terms of Tertiary igneous rocks only.

The magnetic gradient extending from east to west across the aeromagnetic map, indicating the edge of the causative structure, provided an opportunity to investigate some of the geometric parameters of the pluton. Depth to the top of the regional body was

determined on the basis of anomaly amplitude assuming a susceptibility of .003450 cgs units. Anomaly amplitude was quite insensitive to thickness of the pluton for thicknesses exceeding 3 miles. The ratio of negative closure to total anomaly amplitude was sensitive to edge angle and dictated an edge with a dip of 80 to 90 degrees.

With the parameters of depth of burial and edge angle assigned, the separation of the maximum and minimum of the anomaly indicated an approximate thickness of 5 miles for the pluton. The anomaly computed over a "bottomless" pluton, represented by a model 12 miles thick, the assumed depth of the Curie point isotherm (Vacquier and Affleck, 1941), clearly did not fit the observed data (figure 12).

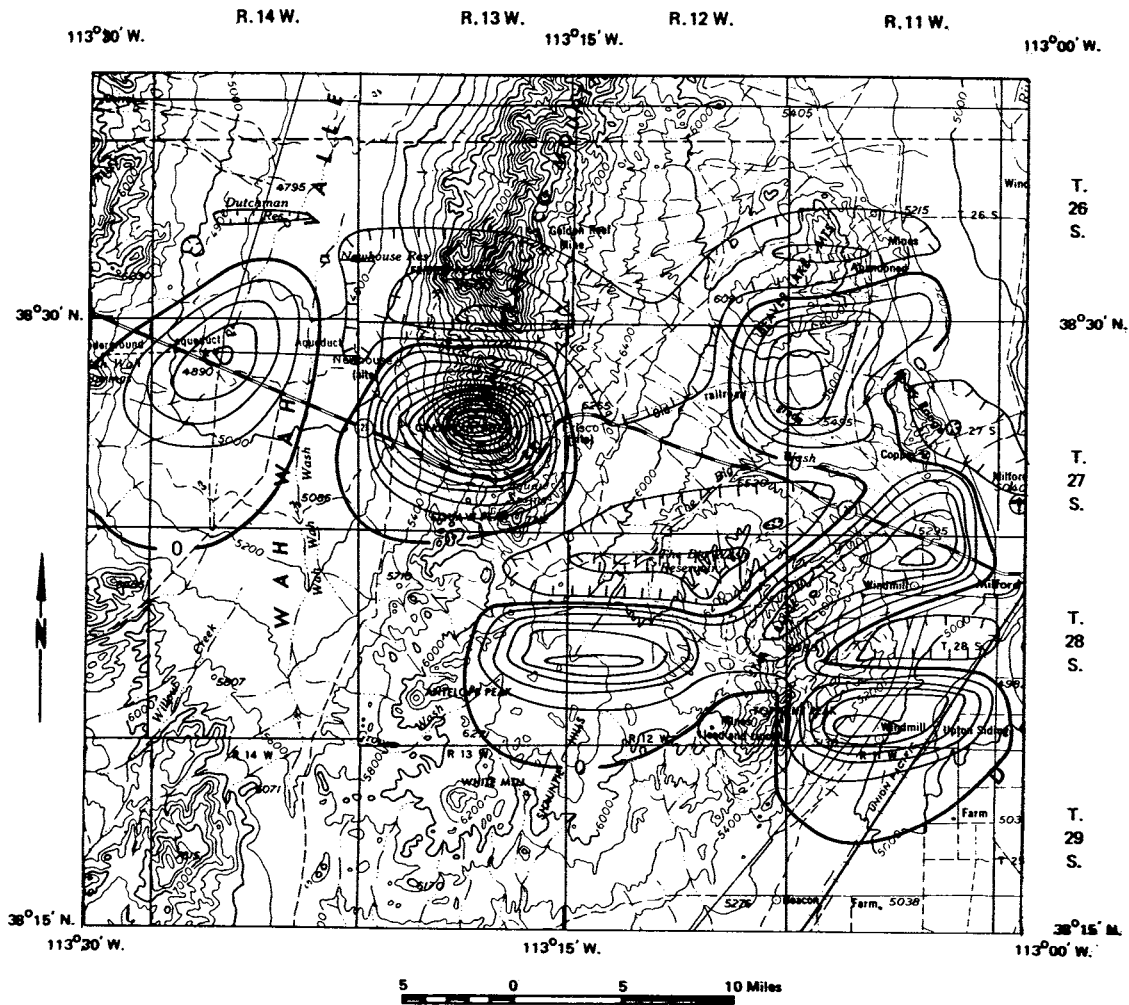


Figure 10. Total-intensity magnetic field generated by the residual igneous model. Values were computed at an elevation of 9,000 feet. This figure should be compared to figure 6. Contour interval = 40 gammas.

The north edge of the pluton extends east-west with minor inflections. This trend is not only discordant with Basin and Range structure, but with other structures in the region dating from Late Precambrian time. Mabey and Morris (1967), however, note that in the Tintic Valley and vicinity, some 100 miles north of the San Francisco Mountains area, igneous rocks and related magnetic anomalies occur in a broad west-trending belt. Farther north, the Bingham, Alta and Park City intrusive belt has an east-west alignment (Mabey and others, 1964). These two areas of igneous activity together with the Milford area account for 95 percent of the copper, lead, silver, gold and zinc produced in Utah (Hilpert and Roberts, 1964).

The full extent of the plutonic body underlying the study area is not shown by the aeromagnetic map.

The outcrop pattern of intrusive rocks in southwest Utah (figure 13; Cohee and others, 1962) indicates that the San Francisco Mountains area may be part of an intrusive belt which extends about 85 miles in an east-west direction and is some 20 miles wide.

The absence of major surface structures coincident or parallel to the belts of intrusive rocks in western Utah suggests that the gross configurations of the belts may be controlled by pre-existing, deep-seated structures only indirectly related to upper crustal structure (Mabey and Morris, 1967). Fuller (1964) discussed magnetic anomaly patterns in parts of the western United States which appear to be interrupted by east-west features, and considers the interruptions to be an expression of deep fracture patterns, partly decoupled from the upper crust.

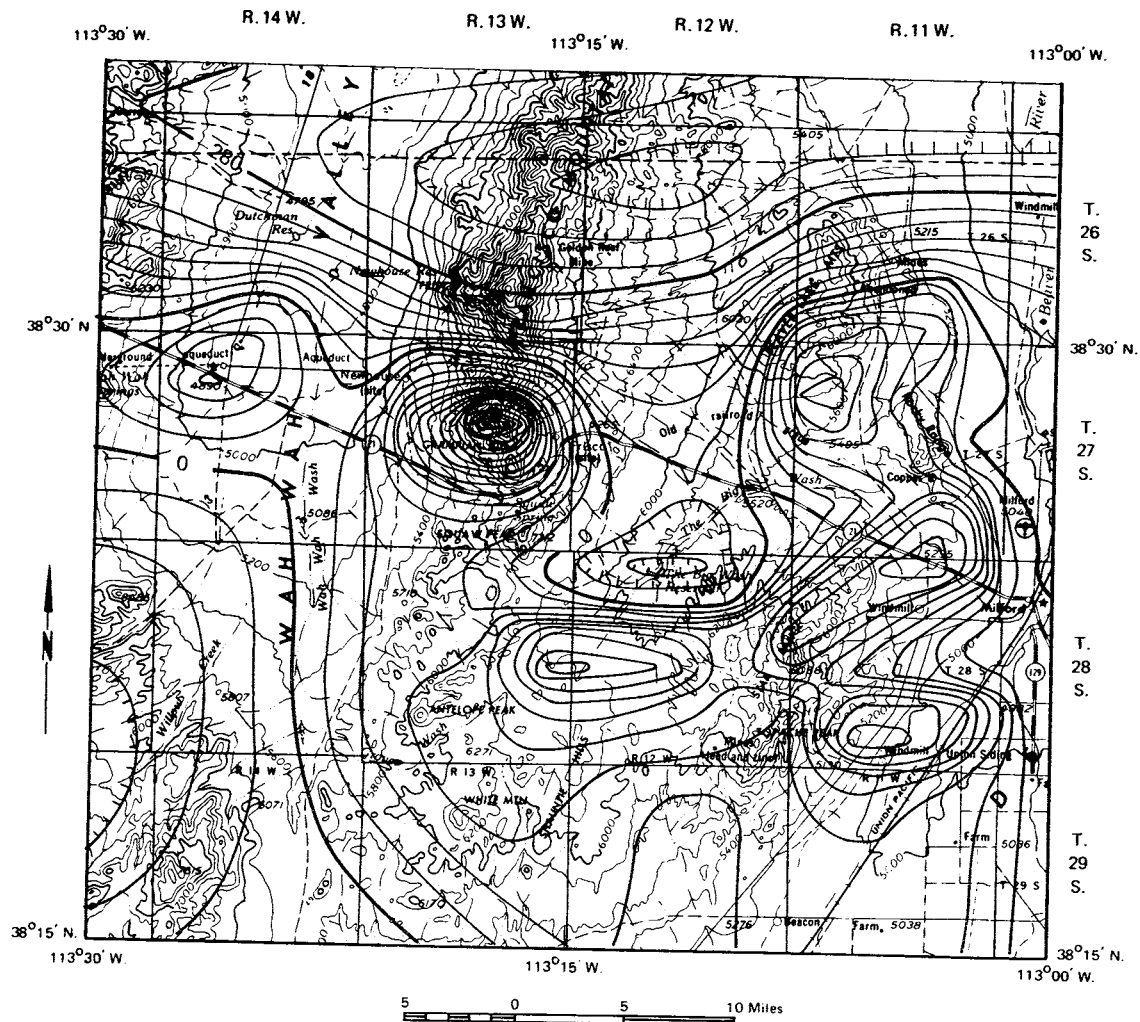


Figure 11. Total-intensity magnetic field generated by the total igneous model. This figure is the sum of the data of figures 9 and 10 and should be compared to figure 3. Contour interval = 40 gammas.

GRAVITY SURVEY

Introduction

Reconnaissance gravity surveys in the San Francisco Mountains area were carried out by the U. S. Geological Survey. Gravity data analyzed in this study were obtained from an open-file, complete Bouguer-gravity map (USGS, 1966b), contoured from 390 gravity stations and covering the same area as the aeromagnetic survey. The Bouguer anomalies were computed by the U. S. Geological Survey for a sea level datum using a density of 2.67 grams per cc. Terrain corrections using the same density were made by the method of Hammer (1939). The gravity values have an estimated uncertainty of 2 milligals. The Bouguer anomaly map was digitized at 1-mile intervals to obtain data on a grid for subsequent computer analysis.

The gravity data contain the effects of both deep-seated, regional geologic structures and more local, near-surface structures. The running average method for separating regional and local anomalies, used for the aeromagnetic data, also was applied to the gridded Bouguer anomaly map of the San Francisco Mountains area. A 13*13 running average was selected as best separating local and regional effects. Figures 14 and 15 are the residual and regional gravity maps produced by this method.

Observations (Residual Gravity Map)

Over most of Nevada and western Utah, the dominant Bouguer gravity anomalies are produced by the density contrast between pre-Tertiary rocks and less dense, younger volcanic and sedimentary rocks (Mabey, 1960). The largest anomalies are located over

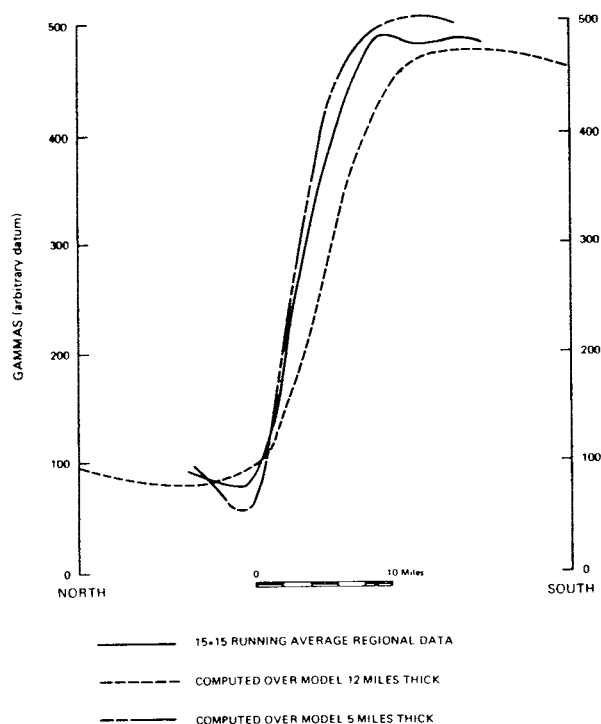


Figure 12. Comparison of observed regional aeromagnetic data and the anomalies computed over horizontal plates with thicknesses of 5 and 12 miles.

basins underlain by thick accumulations of low-density clastic material. Local intermontane anomalies associated with density contrasts in the pre-Tertiary rocks and between Tertiary intrusive and pre-Tertiary rocks are of much smaller amplitude (Mabey, 1960).

In the San Francisco Mountains vicinity, residual gravity highs and lows correlate well with topography, since Basin and Range orogenic activity has been the controlling influence on the region's present morphology. The gravity map confirms some of the structural features seen on the geologic map (figure 2) and indicates a continuation of some structural units beneath alluvial or volcanic cover.

On the westernmost edge of the region, the east foothills of the Wah Wah Mountains are present. The Wah Wah Range is an uplifted and tilted fault block dipping gently eastward into the downfaulted Wah Wah graben (Mackin, 1960a). This structural transition is represented on the residual Bouguer anomaly map by a gradient of about two to three milligals/mile along the west border.

The San Francisco Mountains are part of a north-south trending, uplifted structural block, also dipping to the east (Mackin, 1960a). The well defined structural transition from the Wah Wah graben to the San

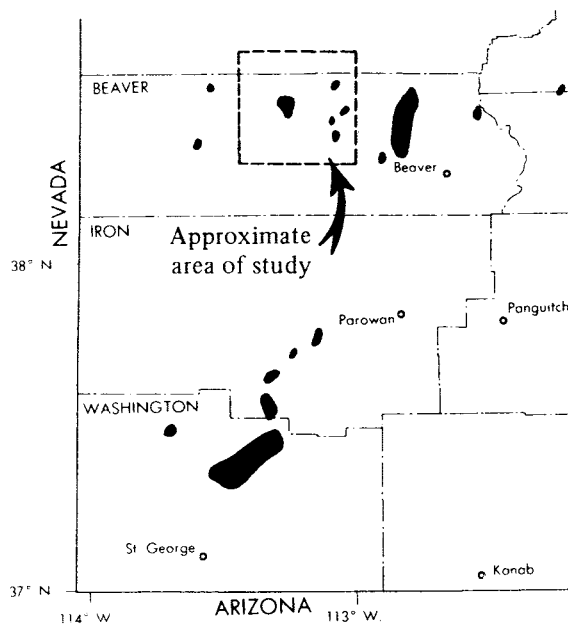


Figure 13. Outcrop pattern of intrusive rocks in southwestern Utah.

Francisco Mountains is represented on figure 14 by a gradient of about 5 milligals/mile. The residual map indicates that the basic structural block of the San Francisco Mountains extends southward under the volcanics shown on figure 2 to at least the south map edge. Several small windows in the volcanic rocks in this area reveal Paleozoic rocks. A small gravity low located 7 miles from the south map boundary may represent either an area where the lower-density volcanic rocks thicken considerably or a small down-faulted area which filled with alluvium prior to being covered by volcanics.

Farther to the east, the Beaver Lake Mountains, the Rocky Range and the Star Range represent high points along an uplifted structural block. The geologic map shows alluvium between these ranges and between the Beaver Lake Mountains and the San Francisco Mountains, but the gravity data indicate that this alluvium does not represent thick accumulations of basin fill.

In the east central portion of the residual gravity map, a gravity low is flanked on the west and east by the gravity highs corresponding to the San Francisco Mountains and the Beaver Lake-Rocky-Star Group. This gravity low represents a small graben structure, herein called the Big Wash graben.

On the east edge of the residual map a gradient of about 5 milligals/mile represents the deepening of

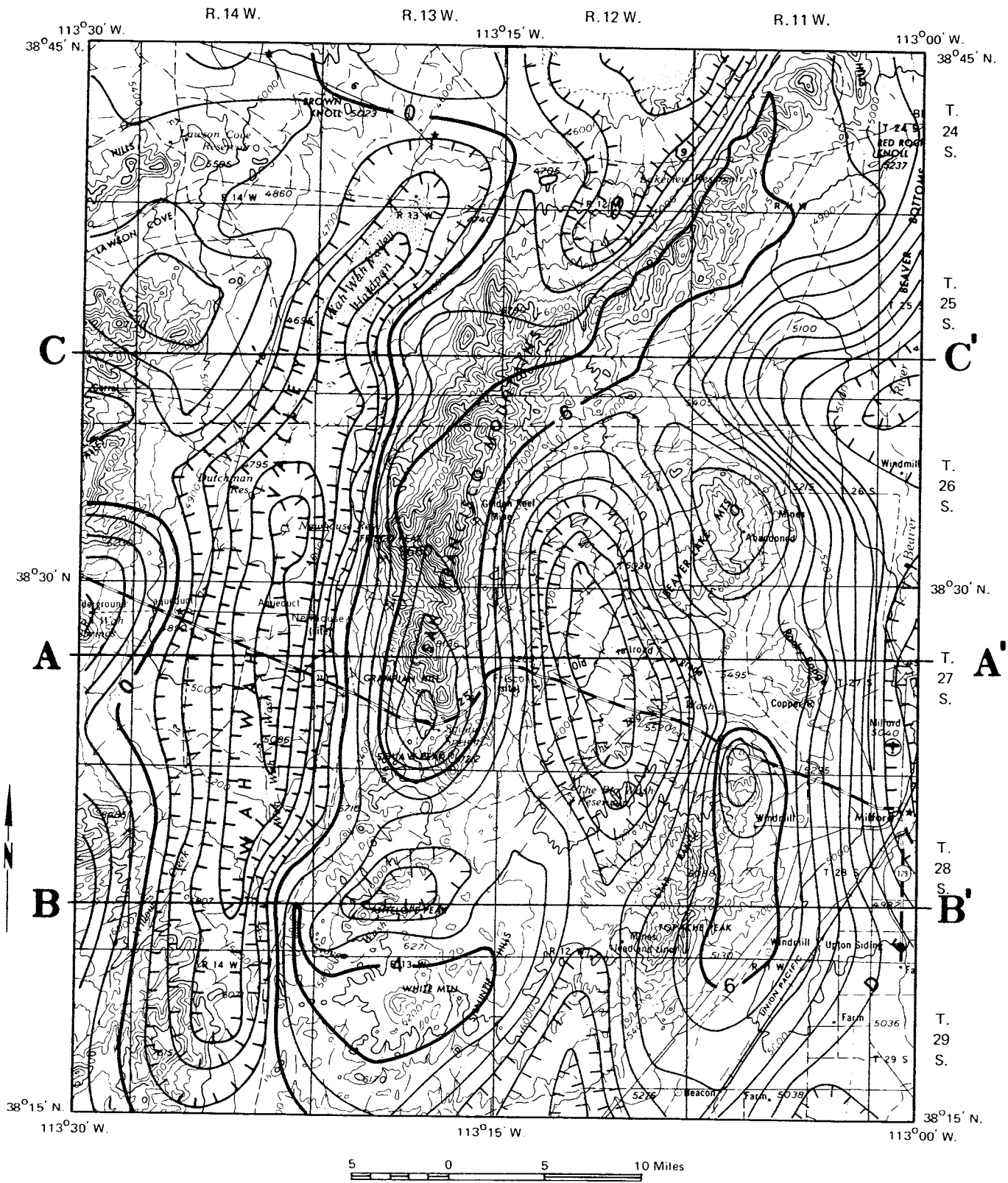


Figure 14. 13*13 running average residual map of the Bouguer anomaly gravity data, San Francisco Mountains vicinity. Contour interval = 40 gammas.

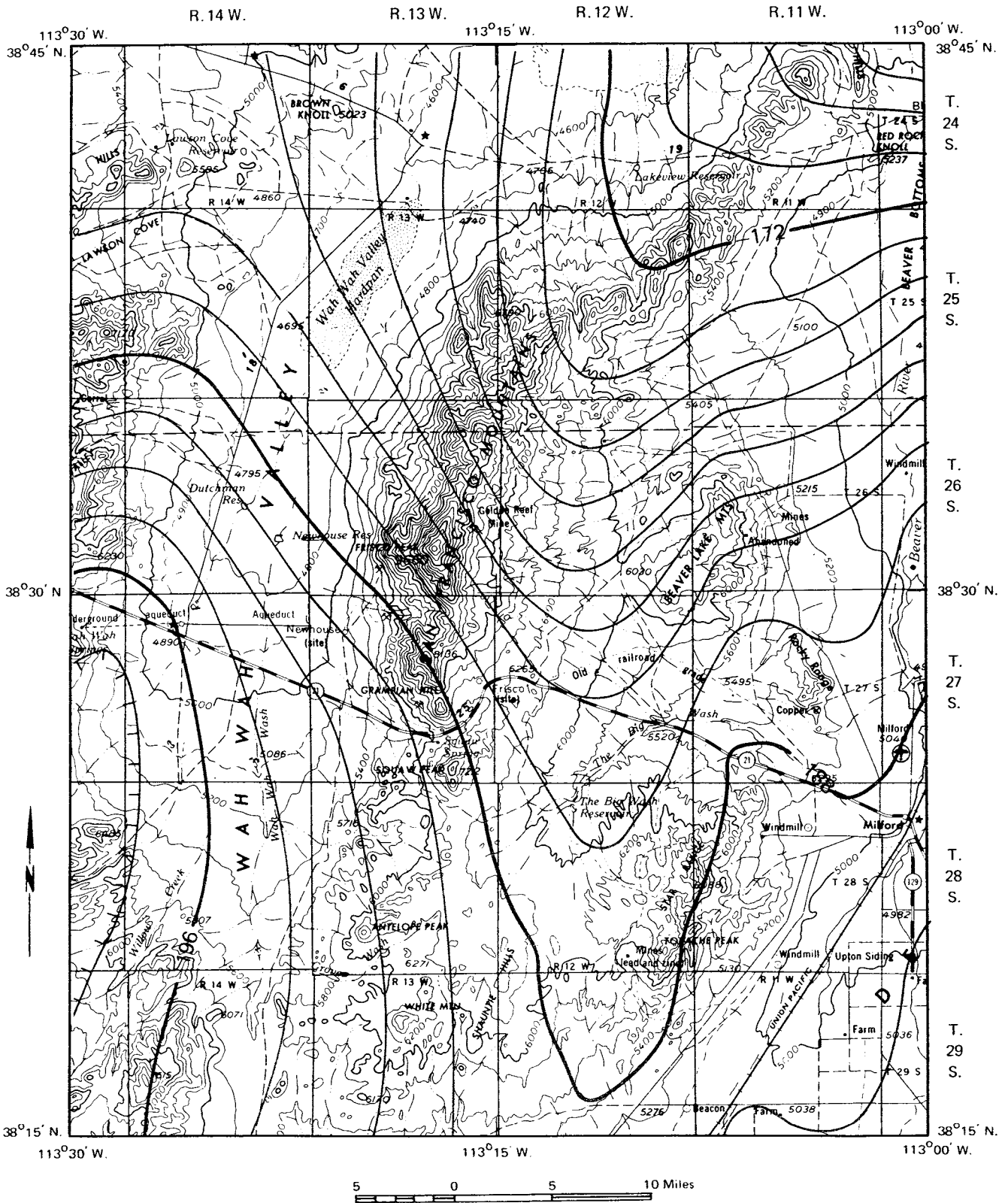


Figure 15. 13*13 running average regional map of the Bouguer anomaly gravity data, San Francisco Mountains vicinity. Contour interval = 40 gammas.

alluvial fill on the west edge of the Milford Valley graben. The graben is about 12 miles wide and contains 5,500 feet of fill at its deepest point (Cook and Mudgett, 1966).

Interpretation of Selected Residual Gravity Profiles

The geologic structures represented by the residual gravity data (figure 14) have pronounced north-south alignments. Three east-west residual gravity profiles extending across the map were selected as representative of the region. The locations of the profiles—AA', BB' and CC'—are shown on figures 2 and 14.

Gravity profiles computed over two-dimensional geologic models (after the method of Talwani and others, 1959), were compared to the data. In keeping with the reconnaissance nature of the data, the models used were geometrically simple. Models were developed to reproduce the residual profiles to within 2 milligals, the approximate precision of the gravity data.

Along a typical east-west profile across the study area, the topographic relief could exceed 3,500 feet. If computed data are to be compared to observed data, the computed gravity effect of a model should be calculated on the actual topographic surface and not on a plane. This is especially important when the causative body extends above some points of observation. Consequently, Talwani's method was modified to compute the gravity effect of a two-dimensional model on the actual topographic surface.

Figure 16 shows the residual gravity profile AA', the surface geology along the profile and a scale drawing of a two-dimensional model which would explain the residual gravity profile. Also included are the regional gravity profile taken from figure 15 and the residual gravity values (shown by dots) at all gravity station locations within 1.5 miles of profile AA'.

Profile AA' includes the Wah Wah graben, the Big Wash graben and the west part of the Milford Valley graben. An assumed density contrast of -0.45 grams per cc for these grabens is sufficient to explain their gravity anomalies. This density contrast is consistent with that used in other gravity studies in the Basin and Range Province (Mabey and Morris, 1967).

Profile AA' also crosses the intrusive outcrop of the Rocky Range and the intrusive body which outcrops near the Horn Silver mine in the San Francisco Mountains. The residual gravity data along this profile require a positive density contrast of 0.10 grams per cc

between Tertiary intrusive rocks and consolidated Paleozoic sediments. This implies a density of about 2.80 grams per cc for the Tertiary intrusive rocks, which is at the upper limit of the density range given by Carlson and Mabey (1963). Failure to include such a density contrast for the intrusive rocks results in an inadequate explanation of the residual profile (figure 16). The geometry of the models for the intrusive cupolas, as shown in figure 16, is consistent with and constrained by the residual igneous models developed in the interpretation of the aeromagnetic data.

Figure 17 shows the data pertinent to residual gravity profile BB'. BB' was a complicated profile requiring six causative bodies in the geologic model. The model for the Milford Flat intrusive was based on the residual igneous model of figure 9 and assigned a density contrast of +0.10 grams per cc, which was sufficient to explain the residual gravity data. The Wah Wah and Milford Valley grabens are continuations of the structures shown on profile AA' and were represented by models with density contrasts of -0.45 grams per cc.

The central portion of profile BB' traverses a volcanic plateau about 600 feet higher than the surrounding area. This plateau was represented in the model by a layer approximately 600 feet thick of density contrast -0.25 grams per cc (Carlson and Mabey, 1963), which represented volcanic material and gave the necessary gravity effect.

A residual gravity minima just east of the Wah Wah graben may correspond to a thickening of the volcanic layer to a thickness of about 3,700 feet. An alluvium-filled graben beneath the volcanic layer also could cause the gravity low. Similarly, another residual gravity low over the east half of the volcanic layer appears related to the south part of the Big Wash graben and could represent either a thickening of volcanic cover or low-density clastic material under the volcanic layer. Both interpretations imply normal faulting which created a structural depression prior to deposition of the volcanics. The models of figure 17 represent clastic-filled grabens under the volcanic layer. A structural depression was thought most likely to fill with alluvial material as it was formed.

The data for profile CC' are shown in figure 18. Only two causative bodies comprise the structural model: the north part of the Wah Wah graben and the Milford Valley graben. The profile traverses an exposure of Precambrian rock, but a corresponding model with a positive density contrast was unnecessary. The Geological Map of Southwest Utah (Hintze, 1963) describes these Precambrian rocks as "undifferentiated

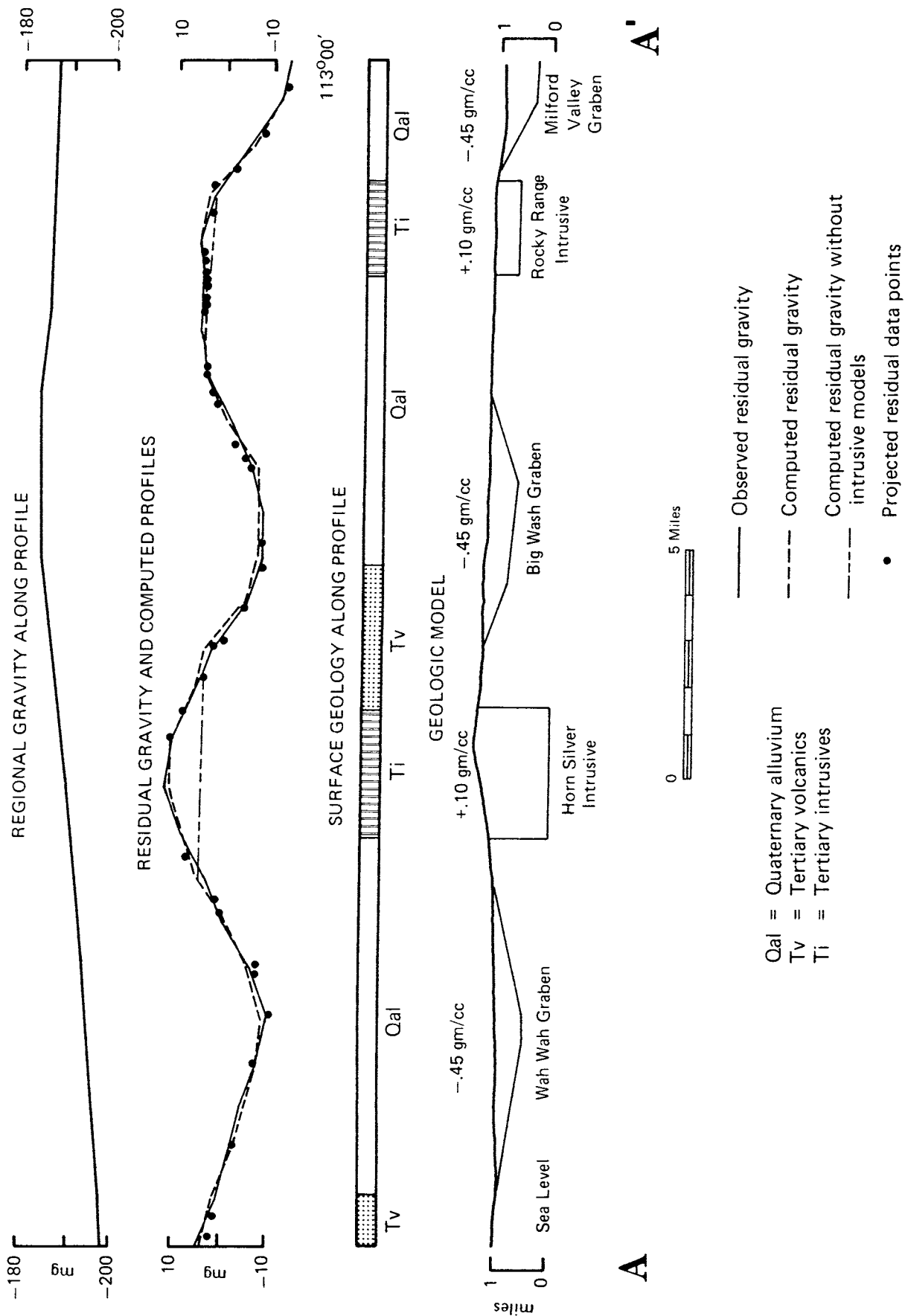


Figure 16. Residual gravity profile AA'.

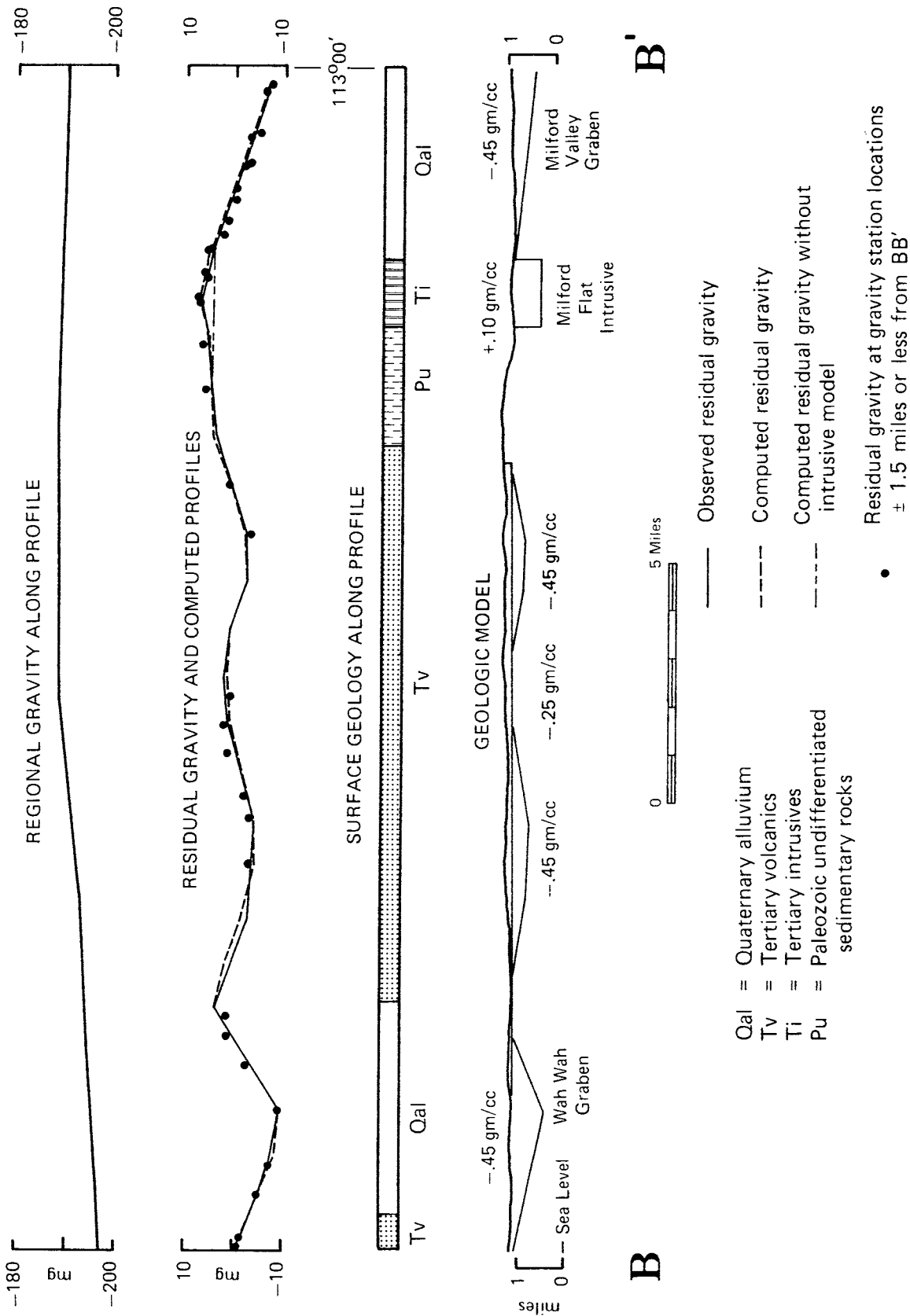


Figure 17. Residual gravity profile BB'.

metasedimentary rocks, chiefly quartzite and argillite, Late Precambrian." They have no expression on the aeromagnetic map.

Table 2 summarizes the maximum depths of fill of the major grabens found along profiles AA', BB' and CC'.

Large areas of the region are covered by volcanics, and since considerable post-volcanic normal faulting is likely, the downfaulted basins probably contain volcanic rocks. Because of the great uncertainty in the thickness and position of volcanic rocks in the grabens, no volcanic layers were included in the graben models. Volcanic rocks would probably be more dense than the clastic material assumed to fill the grabens and their actual presence in a graben would cause the computed depth of fill to be too small—an error which could amount to about 400 feet for a volcanic layer 1,000 feet thick.

The dip of the walls of the graben models is less than 30 degrees. Since the typical graben is probably bounded by a series of faults rather than a single fault plane, the models represent the gross configuration of the graben walls and not the dip of individual fault planes.

Relative Age of Intrusive Emplacement

The regional igneous model (figure 7) representing the underlying intrusive body was determined solely from aeromagnetic data. The model appears to reflect in some measure, however, the block faulting inferred from the residual gravity data. In particular, the generally elevated blocks (2) and (3) of the igneous

Table 2. Maximum depths of fill for the Wah Wah, Big Wash and Milford Valley grabens, as determined from gravity data.

Profile	Maximum depth of fill (feet)
Wah Wah Graben	
AA'	3,200
BB'	3,600
CC'	2,700
Big Wash Graben	
AA'	3,000
BB'	1,200
	(from bottom of volcanics)
Profile	Depth of fill at east edge of map
Milford Valley Graben	
AA'	3,500
BB'	2,500
CC'	3,400

model correspond with the position of the Beaver Lake-Rocky-Star chain of positive structural features, and block (5) corresponds to a structural saddle indicated by the gravity data at the south end of the Big Wash graben. The termination of block (4) towards the west occurs near the east margin of the Wah Wah graben. None of the cupola-like intrusive bodies of figure 9 is intruded into grabens. The evidence is consistent with the assumption that major Basin and Range faulting has occurred after intrusion of the pluton.

Interpretation of Regional Gravity Anomalies

Figure 15 shows the regional gravity map obtained from the gridded Bouguer anomaly data and tends to represent the approximate gravity effects of deep anomaly sources. The regional gravity map has three dominant features:

1. A gradient in the north part of the map increasing towards the north.
2. A gradient in the southwest quadrant of the map decreasing towards the west.
3. A positive nose coinciding with the position of the main horst structure in the area.

Since analysis of the residual gravity data indicates a positive density contrast between near-surface intrusive rocks and consolidated sedimentary rocks, it is reasonable to examine the regional gravity data for evidence of the large intrusive body suggested by the aeromagnetic data. This was done using the method of Talwani and Ewing (1960) for computing gravity effects of three-dimensional mass distributions. The gravity effect of the regional igneous body was computed assuming a density contrast of +0.10 grams per cc with the rocks into which it was intruded. This computed field was subtracted from the regional gravity map.

Figure 19 shows that removal of a positive gravity effect attributed to the underlying pluton greatly exaggerates the gradient which increases to the north, but eliminates the gradient in the southwest quadrant which decreases to the west. The positive nose still can be observed. This implies that the gradient decreasing to the west may be the result of the westward-increasing depth of the intrusive body. The distorted northward-increasing gradient shows that the gravity effect of the pluton alone is not sufficient to explain the regional gravity field.

The near-vertical and generally linear north edge of the regional igneous model suggests the presence of an east-west fault zone extending across the area. This

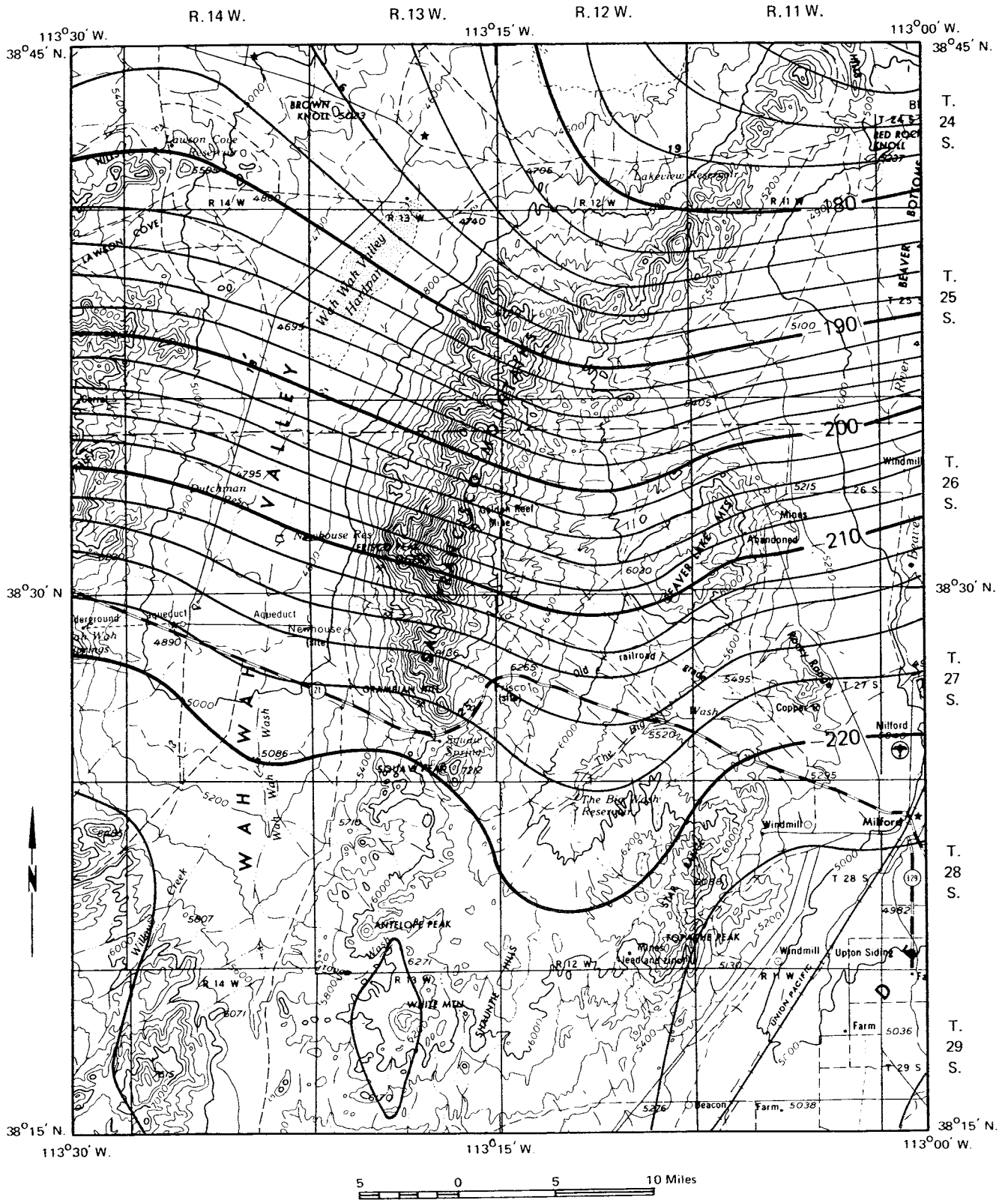


Figure 19. Regional gravity data with the postulated gravity effect of the regional intrusive body removed. Contour interval = 2 milligals.

postulated fault zone permits the introduction of a density contrast between the north and south parts of the map area, which could tend to reproduce the strong regional gravity gradient of figure 19.

Consequently, the gravity effect of a single, vertically sided, horizontal plate was computed using the three-dimensional gravity computation program (Talwani and Ewing, 1960). The plate extended well beyond the map area to the west, north and east and was bounded on the south by the regional intrusive body. The plate was 7 miles thick; the elevation of its top was 1,560 feet below sea level and it had a density contrast of +0.10 grams per cc with the sedimentary rocks on the south side of the postulated fault. Figure 20 shows the relationship of this plate to the regional intrusive model. This simple plate model represents the possibility of differing lithologies on each side of the postulated east-west fault zone.

The gravity effect of this plate was subtracted from the field of figure 19. The resulting map (figure 21) shows the regional gravity data with the possible gravity effects of both the regional intrusive body and the postulated fault zone removed. In figure 21 the strong gradient increasing to the north is no longer present. The remaining gravity contours define a positive nose, coinciding with the position of the main horst structure in the area.

The plate model of figure 20 was designed on the arbitrary assumption of no density contrast between the plate and the intrusive pluton and is presented only as one possible example. More generally, the regional gravity data show an east-west gradient with a total relief of about 14 milligals. Assuming this gradient to be caused by a mass excess on the north side of the postulated fault zone, whose actual distribution is unknown, the mass excess can be described in terms of a surface density. The net amplitude of the gravity anomaly, presumably the result of a differing lithology on the north side of the postulated fault zone, can be approximated by the expression for the gravity effect of an infinite horizontal slab:

$$\Delta g = .01277\delta L$$

where δ is the density contrast of the slab in grams per cc, L the thickness of the slab in feet and Δg the gravity effect in milligals. Setting Δg equal to 14 milligals, $\delta L = 1,100$ gm ft/cc, the surface density over the north side of the fault zone. Within this constraint, various combinations of density contrast and plate thickness can be assumed.

If the supposed fault predates the emplacement of the intrusive body, the positive density contrast

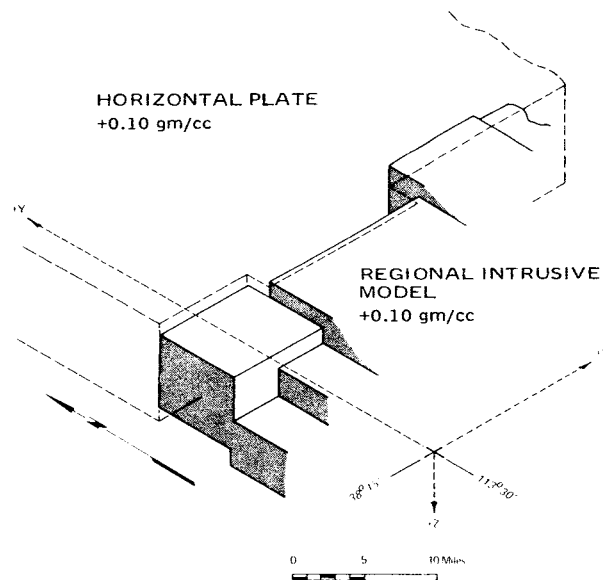


Figure 20. Sketch showing the relationship of the regional intrusive model (from figure 7) to the horizontal plate representing the north side of the postulated east-west fault zone. Only the area of contact between the two structures is shown.

across the fault zone could have acted as a barrier preventing the intruding magma from migrating northward and thus could have controlled the configuration of the north edge of the pluton. If the fault postdates the intrusive body and the pluton is terminated by displacement along the fault, the time of fault displacement would have to fall between the time of pluton emplacement and the start of major Basin and Range faulting, since the horst and graben structures appear unaffected by displacement on the supposed fault zone. Termination of the 5-mile thick pluton by faulting would seem to require a strike-slip fault of at least 30 miles displacement. Lacking additional evidence in the form of field studies or regional aeromagnetic data, the hypothesis that the fault predates the intrusive seems more likely.

The regional gravity high still apparent on figure 21 extends across the postulated east-west fault zone and coincides with a major horst structure. Basin and Range normal faulting appears to postdate the supposed fault zone. This gravity high most likely reflects the deeper density contrasts associated with Basin and Range structure.

Cook and Mudgett (1966) observed a regional gravity high in this general area corresponding in position to the Sevier arch (Harris, 1959), later referred to as the Sevier Orogenic Belt of pre-Laramide age (Armstrong, 1968). The regional gravity high of figure 21 does coincide with the general location of the

Sevier Orogenic Belt and could possibly be caused, in some measure, by the deep-seated structure of the Sevier Belt.

SUMMARY AND CONCLUSIONS

To present the potential field data in a form more readily associated with geologic causative structures, the observed data are separated into regional and residual components by the method of running averages. Interpretation is aided by machine computation of the gravity and magnetic fields generated by models of the proposed causative structures. The models, which are of simple geometry, provide insight into the regional geology, but could differ significantly from the actual configuration of the causative structures. The gravity or magnetic expression of mineralization or related processes is not recognized on the data, and such effects, if present, are presumably within the error limits of model reproduction of observed data.

On the basis of the aeromagnetic data and model studies, it is concluded that the study area is underlain by a large Tertiary intrusive pluton, whose north boundary runs from east to west across the north portion of the map, and which extends beyond the coverage of the aeromagnetic map to the east, south and west. The elevation of the top of the pluton decreases from about 2,000 feet above sea level in the east to about 11,000 feet below sea level in the west, and local intrusive cupolas extend upward from the main igneous body. The pluton is distinctly tabular with a more or less uniform thickness of 5 miles and has a vertical or near-vertical north edge.

From west to east across the map area, the gravity data delineate the east edge of the Wah Wah Mountains, Wah Wah graben, San Francisco Mountains, Big Wash graben, Beaver Lake-Rocky-Star ranges and the west edge of the Milford Valley graben.

Three interpretive east-west cross sections of the residual gravity data are developed. The Wah Wah graben has an interpreted maximum thickness of fill of 3,600 feet, while the Big Wash graben has a maximum thickness of fill of about 3,000 feet. At the east edge of the map area, the Milford Valley graben has a thickness of fill ranging from 2,500 to 3,500 feet. To adequately explain the residual gravity data, a positive density contrast of approximately 0.10 grams per cc must be assumed for the near-surface intrusive cupolas. Two small gravity lows along profile BB' occur over volcanic rock and are interpreted as representing either thickening of the volcanic cover or clastic-filled depressions under the volcanics.

The regional gravity map is interpreted, with the help of a three-dimensional gravity computation program, as reflecting the gravity effect of three and possibly four regional structures:

1. An underlying intrusive body.
2. An east-west fault zone bounding the intrusive body on the north.
3. Deep-seated Basin and Range horst and graben structure.
4. Possibly the Sevier Orogenic Belt.

ACKNOWLEDGMENTS

The author is indebted to E. S. Robinson for helpful discussions and guidance. The University of Utah and Virginia Polytechnic Institute made computer time available. During 1966 and 1967 the author was a recipient of a NASA fellowship; other financial assistance was given by the Geophysics Department, University of Utah, and the Department of Geological Sciences, Virginia Polytechnic Institute.

REFERENCES

- Affleck, J., 1963, Magnetic anomaly trend and spacing patterns: *Geophys.*, v. 28, p. 379.
- Armstrong, R. L., 1968, Sevier Orogenic Belt in Nevada and Utah: *Geol. Soc. Am. Bull.*, v. 79, p. 429.
- Blank, H. R. and J. H. Mackin, 1967, Geologic interpretation of an aeromagnetic survey of the Iron Springs district, Utah: *U. S. Geol. Survey Prof. Paper 516-B*.
- Boardman, L., compiler, 1954, Geologic map index of Utah: *U. S. Geol. Survey*.
- Butler, B. S., 1913, Geology and ore deposits of the San Francisco region, Utah: *U. S. Geol. Survey Prof. Paper 80*.
- Butler, B. S. and others, 1920, Ore deposits of Utah: *U. S. Geol. Survey Prof. Paper 111*.
- Carlson, J. E. and D. R. Mabey, 1963, Gravity and aeromagnetic investigations of the Ely area, Nevada: *U. S. Geol. Survey Geophys. Inv. Map GP-392*.
- Cohee, G. V. and others, 1962, Tectonic map of the United States: *U. S. Geol. Survey and Am. Assoc. Petroleum Geologists*.
- Cook, K. L. and P. M. Mudgett, 1966, Regional gravity survey of the Mineral, San Francisco, Beaver and northern Wah Wah Mountains region, in Beaver and Millard counties, Utah (abs): *Utah Acad. Proc.*, v. 43, pt. 2, p. 62.
- Davis, W. M., 1925, The Basin Range problem: *Natl. Acad. Sci. Proc.*, v. 11, p. 387.

- Doell, R. R. and A. Cox, 1962, Determination of the magnetic polarity of rock samples in the field: U. S. Geol. Survey Prof. Paper 450-D, p. 105.
- Eardley, A. J., 1962, Structural geology of North America, 2nd ed.: New York, Harper and Row, 743 p.
- Fuller, M. D., 1964, Expression of E-W fractures in magnetic surveys in parts of the U. S. A.: Geophys., v. 29, p. 602.
- Gilbert, G. K., 1874, Progress report of U. S. Geological Surveys, west of the 100th meridian for 1872: U. S. Geol. Survey, p. 50.
- _____, 1928, Studies of Basin Range structure: U. S. Geol. Survey Prof. Paper 153.
- Hammer, S., 1939, Terrain corrections for gravimeter stations: Geophys., v. 4, p. 184.
- Harris, H. D., 1959, A late Mesozoic positive area in western Utah: Am. Assoc. Petroleum Geologists Bull., v. 43, p. 2636.
- Hilpert, L. S. and R. J. Roberts, 1964, Economic geology, in Mineral and water resources of Utah: Utah Geol. and Mineralog. Survey Bull. 73, p. 28.
- Hintze, L. F., compiler, 1963, Geologic map of southwestern Utah: Utah Geol. and Mineralog. Survey.
- Jaffe, H. W. and others, 1959, Lead-alpha age determinations of accessory minerals of igneous rocks (1953-1957): U. S. Geol. Survey Bull. 1097-B.
- Mabey, D. R., 1960, Regional gravity survey of part of the Basin and Range Province: U. S. Geol. Survey Prof. Paper 400-B, p. 283.
- Mabey, D. R. and others, 1964, Aeromagnetic and generalized geologic map of part of north central Utah: U. S. Geol. Survey Geophys. Inv. Map GP-422.
- Mabey, D. R. and H. T. Morris, 1967, Geologic interpretation of gravity and aeromagnetic maps of Tintic Valley and adjacent areas, Tooele and Juab counties, Utah: U. S. Geol. Survey Prof. Paper 516-D.
- Mackin, J. H., 1960a, Structural significance of Tertiary volcanic rocks in southwestern Utah: Am. Jour. Sci., v. 258, p. 81-131.
- _____, 1960b, Eruptive tectonic hypothesis for origin of Basin-Range structure (abs): Geol. Soc. Am. Bull., v. 71, p. 1921.
- Moore, J. G., 1960, Curvature of normal faults in the Basin and Range Province of the western United States: U. S. Geol. Survey Prof. Paper 400B, p. 409.
- Nettleton, L. L., 1954, Regionals, residuals and structures: Geophys., v. 19, p. 1.
- Nolan, T. B., 1943, The Basin and Range Province in Utah, Nevada and California: U. S. Geol. Survey Prof. Paper 197-D, p. 141.
- Roberts, R. J. and others, 1958, Paleozoic rocks of north central Nevada: Am. Assoc. Petroleum Geologists Bull., v. 42, p. 2813.
- Roberts, R. J., 1960, Paleozoic structure in the Great Basin (abs): Geol. Soc. Am. Bull., v. 71, p. 1955.
- Skeels, D. C., 1947, Ambiguity in gravity interpretation: Geophys., v. 12, p. 43.
- Talwani, M. and others, 1959, Rapid gravity computations for two-dimensional bodies with application to the Mendocino submarine fracture zone: Jour. Geophys. Res., v. 64, p. 49.
- Talwani, M. and M. Ewing, 1960, Rapid computation of gravitational attraction of three-dimensional bodies of arbitrary shape: Geophys., v. 25, p. 203.
- Talwani, M., 1965, Computation with the help of a digital computer of magnetic anomalies caused by bodies of arbitrary shape: Geophys., v. 30, p. 797.
- U. S. Coast and Geodetic Survey, 1955, Total intensity chart of the United States: U. S. Coast and Geodetic Survey Chart 3077f.
- U. S. Geological Survey, 1966a, Aeromagnetic map of the San Francisco Mountains and vicinity, southwestern Utah: U. S. Geol. Survey Geophys. Inv. Map GP-598.
- _____, 1966b, Complete Bouguer gravity anomaly map of the San Francisco Mountains vicinity, Beaver and Millard counties, Utah: U. S. Geol. Survey, Open-file map No. 482G.
- Vacquier, V. and J. Affleck, 1941, A computation of the average depth to the bottom of the earth's magnetic crust based on a statistical study of local magnetic anomalies: Trans. Am. Geophys. Union, v. 22, Ann. Mtg., pt. 2, p. 446.
- Vestine, E. H. and others, 1947, Description of the earth's main magnetic field and its secular change, 1905-1945: Carnegie Inst. Washington Publ. 578, p. 532.